To be published in IEEE Trans.
Nuclear Science

LBL-338
Preprint c.1

A LIQUID XENON RADIOISOTOPE CAMERA

Haim Zaklad, Stephen E. Derenzo, Richard A. Muller,
Gerard Smadja, Robert G. Smits, and Luis W. Alvarez

February 1972

AEC Contract No. W-7405-eng-48

A LIQUID XENON RADIOISOTOPE CAMERA

Haim Zaklad, Stephen E. Derenzo, Richard A. Muller,*
Gerard Smadja, Robert G. Smits, and Luis W. Alvarez

Lawrence Berkeley Laboratory
University of California
Berkeley, California

*Space Sciences Laboratory
University of California
Berkeley, California

1. Summary

The increasing availability of short lived gamma and positron emitting isotopes, coupled with the importance of dynamical studies and better imaging, has generated the need for an improved γ-ray camera.

We discuss a new type of γ-ray camera which makes use of electron avalanches in liquid xenon. A configuration currently under development is shown in Fig. 1.

The successful operation of a liquid xenon proportional counter was recently reported.[1] The liquid xenon camera promises better spatial resolution and higher counting rate than the existing NaI(Tl) scintillation camera. The spatial resolution for γ rays is in principle limited only by the range of photoelectrons in liquid xenon, which is < 0.2 mm for energies < 1 MeV. A counting rate of 10^6 C/s or more appears possible. As a result of the better resolution and high counting rate capability, the definition of the picture is improved. In addition, the high counting rate capability makes possible dynamic studies which were previously unfeasible.

Although we expect the energy resolution with liquid xenon to be superior to that of NaI (see next section), our preliminary measurements show 17% FWHM for 279 keV γ's. Improvements are expected by using better geometry and smoother wire.

2. Liquid Xenon as a Detector Medium

Liquid xenon is a well adapted medium for the detection of γ rays due to its high density (3.06 g/cm^3) and its high Z (54). It is the only known liquid in which ionization electrons both remain free and can be avalanched reliably to give a fast electronic pulse.

We have studied the electron avalanche process near fine wires (3.5μ to 25μ-diam) at fields $\geq 10^6$V/cm and a voltages of > 2000 V in pure liquid xenon.[1] The observed pulse rise time of 150 ns for the proportional pulses and ≈ 20 ns for the Geiger-type pulses should permit a counting rate higher than 10^5 counts per second per wire. The detection efficiency for ionizing particles is 100%, and for γ rays is limited by the efficiency of conversion (see Section 4). We measured the average energy required to produce an ion pair in liquid xenon and found a value of 23±2 eV, similar to that in gaseous xenon. The electron drift velocity in liquid xenon is 3×10^5 cm/s at fields > 1000V/cm.[2] Gains of 100 or more result in output pulses of 0.7 pC/MeV (1pC = 10^{-12} coulomb), well within the range of a simplified electronic readout (see Section 7). With a liquid gain of 100, the charge signal is an order of magnitude greater than the signal from a germanium detector. Table 1 compares some of the properties of NaI(Tl), germanium, and liquid xenon detectors

Good pulse height resolution is necessary to reject the γ rays that have scattered within the patient. Because the number of ionization electrons produced by a γ-ray conversion in liquid xenon is an order of magnitude greater than the number of usable photoelectrons from a NaI(Tl) crystal viewed by a photomultiplier, we expect (a priori) the energy resolution of a liquid xenon detector to be superior to that of NaI(Tl). With a collimated beam of 279 keV γ rays (Hg^{203}) incident on a cylindrical chamber we have achieved an energy resolution of 17% (FWHM), whereas 11% is readily attainable with NaI(Tl). We do not yet understand why the resolution is not better; we may be able to improve it by using a different chamber geometry. Figure 2 shows the pulse height spectrum from a collimated Hg^{203} source. The liquid gain is 10 and the FWHM of the 279 keV peak is 22%. With α particles we have achieved a resolution of better than 13% (FWHM).

The detection efficiency of the photoelectrons is especially important when high energy resolution and high spatial resolution are required simultaneously. In the NaI detector, a γ ray that is totally stopped by multiple interactions gives a total pulse height in the photopeak region, even though the center of the flash is away from the original track. Anger computed this distribution for chambers of various thicknesses.[3]

We propose to reject multiple Compton scattering in the liquid xenon by performing pulse height analysis on each wire individually. Thus, at the cost of a somewhat lower detection efficiency, the image will have improved contrast and enhanced spatial resolution, compared to the NaI camera.

The ratio of the photoelectric effect cross section to the total cross section[4,5] is compared in Fig. 3 for NaI, xenon, and germanium. These curves provide a good estimate of the photofraction (fraction of the incident γ's that fall within the photopeak) for a "thin" chamber. We note that this ratio in germanium drops much more rapidly with increasing energy than in either xenon or NaI. As the chamber becomes thicker, the probability for multiple interactions leading to total absorption increases; hence the area under the photopeak increases. Thus, the photofraction for a thick detector is greater than for a thin detector. See Fig. 3 for results with a 2 in thick NaI crystal.[6]

In the positron mode, the blurring of the image due to scattering in the tissue is reduced by accepting only unscattered gammas, and a high counting rate is achieved by the elimination of the collimator. Lavoie showed some advantages of the liquid xenon scintillator for the detection of 500 keV annihilation γ rays.[7] The importance of having a large photofraction is greater in this mode of operation, since a coincidence of two photopeak electrons is required. The number of coincidences is proportional to the square of the photofraction. In thin liquid xenon chambers the photofraction at 500 keV is about five times larger than in germanium.

3. Electronegative Impurities in Liquid Xenon

As the free electrons drift in the liquid under the influence of an electric field, some are lost by attachment to electronegative impurities. After drifting through a distance, x, the fraction surviving is given by

$$\frac{N}{N_0} = e^{-kCx},$$

where

N = Number of electrons surviving capture and reaching the anode
N_0 = Initial number of electrons
x = Distance of travel (mm)
k = Probability of capture per mm of drift per ppm impurity
C = Concentration of electronegative impurities (ppm).

The fraction $\frac{N}{N_0}$ of the number of initial free electrons N_0 that survive attachment and multiply near the anode produce a pulse of magnitude:

$$Q = Q_0 G e^{-kCx},$$

where G is the gain and Q_0 the initial charge. In order to insure the detection of all of the converted γ rays in the liquid, the pulse height due to the electrons must be higher than the detection level of the readout electronics. Electronegative impurities degrade the energy resolution by relating the pulse height to the position of the initial ionization. High purity is therefore essential for good energy resolution, especially in thick chambers. Thick chambers are desired for good conversion efficiency with high energy gamma rays. Impurities could thus limit both the energy resolution and the chamber thickness.

We have found[8] that for oxygen in liquid argon at fields of a few kilovolts per cm, k = 0.26 ± 0.1/ppm/mm. This means, for example, that only 80% of the initial electrons arrive at the anode after traveling in a central anode chamber 1.5 cm thick containing 0.1 ppm O_2. Using techniques described in ref. 8, we have prepared xenon gas that reliably contains less than 50 ppb of oxygen and nitrogen (measured with a Varian helium ionization gas chromatograph). Yet, we have observed that the impurity level in a large size chamber containing liquid xenon sometimes exceeds kC = 1 per mm.

We find no difficulties in consistantly obtaining clean liquid (kC < 0.02) by means of the following 2 stages:

a. Gas purification:[8] The xenon gas continuously circulates, by means of a positive displacement pump, for several hours over a hot copper catalyst (200°C) and cold (-77°C) molecular sieve 4A material (see Fig. 4). The copper reacts with oxygen while the molecular sieve traps other unknown electronegative impurities. Every few weeks of operation, excess nitrogen is removed by passing the gas over hot calcium chips (600°C).

b. Liquid purification by electronegative ion pumping (ENIP): We found ENIP to be an excellent means of further purifying the liquid in the chamber. This is often necessary due to impurities not removed by the purifier and probably introduced by the walls of the chamber or by the purifier. In order to perform this ion pumping, the voltage of the fine wire anode is reversed and becomes negative. As the voltage is raised, the wires emit electrons that are captured by the impurities. The negatively charged impurities that drift to the now positive electrode remain there for several hours, even when the voltage is reversed during the normal mode of operation. If kCx is high, a current of 1μA can remove $10^{-6}/1.6\times10^{-19}$ or $\sim 6\times10^{12}$ molecules/sec. In a typical chamber (5 cm long, 2 mm wire spacing, 1 cm thick) this amounts to ~ 0.2 ppm impurities for 10 minutes of ENIP Typically, 10 to 30 minutes of ENIP are sufficient to provide full expected pulse height. The harmful impurities must be those present in a very small concentration, below the ppm level and with very high k value. There are materials known to have an electron attachment cross-section several thousand times larger than that of oxygen (for example, SF_6).[9] We believe that outgassing is the source of most of such impurities.

4. Calculated Spatial Resolution and Detection Efficiency

We have measured the spatial resolution of liquid xenon chambers to be better than 15μ for alpha particles.[1] For γ rays the resolution is limited in principle by the radial distance traveled by the photoelectrons. For 511 keV annihilation γ rays we have measured the spatial resolution to be better than 1mm rms (see Section 5). In the following section we estimate the ultimate spatial resolution for a gamma ray chamber.

The following scattering processes contribute:
(a) A primary photoelectric interaction in which all of the gamma ray energy is absorbed by a photoelectron. For the energies considered, the error due to the path length of the photoelectron is small (see below). The probability of generating a photoelectron diminishes rapidly with increasing energy.
(b) A single Compton interaction followed by the escape of the secondary gamma ray from the detector.
(c) A Compton interaction, followed by a secondary scattering, may occur at a distance away from the original gamma ray track, and may generate either a photoelectron or another Compton electron.

The gross detection efficiency (Fig. 5) is the sum of the three processes described. This was computed for 0.75, 1.5, and 3 cm thickness of liquid xenon, using the data given by McMaster[4] and Hubbell.[5] The only source of spatial error in processes (a) and (b) is the movement of the conversion electron away from the point of the γ-ray interaction. In xenon, multiple scattering of the electron is so severe that the net distance that the electron travels is only a fraction of its "range". It has been estimated by a Monte Carlo method:[10]

Electron Energy (keV)	100	200	500	1000
Distance from Primary Gamma (mm)	0.012	0.057	0.11	0.21

Thus, at the level of accuracy we want to consider (~ 1mm), the electron recoil effects can be ignored. Furthermore, at lower energies the γ-ray attenuation length decreases so quickly with decreasing energy, that if multiple Compton scattering of the initial photon takes place, the third, fourth, and later interactions are very close to the second one. At higher energies, triple scattering is not as likely. The following computations therefore deal with double scattering only. For a γ ray, incident along the Z direction shown in Fig. 6, we have computed by numerical integration the probable distribution of the secondary scatter:

$$w(y) = \int_0^L \frac{e^{-Z_1/\lambda_1}}{\lambda_1} dZ_1 \int_{-1}^{+1} f(\theta)\, d(\cos\theta)$$

$$\times \int_{Z_1}^{L(\theta)} \frac{e^{-Z_1/\lambda_2 \cos\theta}}{\lambda_2 (Z_2 - Z_1) \sin\theta \cos\eta} \cos\theta \; dZ_2 ,$$

where L is the thickness of the chamber, $\sin\eta = \frac{y}{(Z_2 - Z_1)\tan\theta}$, and λ_1, λ_2 are the attenuation lengths of the primary and scattered photon; $f(\theta)$ is the angular distribution for the scattering, which is given by the standard Klein-Nishina formula. Also, $L(\theta) = (L - Z_1)$ for $\cos\theta > 0$ and $L(\theta) = 0$ for $\cos\theta > 0$. The first integral is the probability for a primary interaction at Z_1; the second integral is the probability for a scattered γ ray in the θ direction; the third integral is the probability of a second interaction at Z_2 times the probability that the second interaction would have a position y when originating from Z_2, θ.

Table 2 and Figs. 7 and 8 summarize the results of the computation for 0.75cm, 1.5cm, and 3.0cm-thick chambers and for the γ-ray energies of 100, 200, 500, and 1000 keV. The gross detection is the probability of interaction of any kind either photoelectric or Compton. The fraction of the various processes, normalized to unity when no energy window is applied, is listed in columns b, c, and d. This normalization is useful in order to show the contrast of the camera picture.

Column b is the fraction of the photoelectric process. Column c is the fraction of a single Compton interaction, followed by an escape from the chamber (never attaining full pulse height). Column d is the fraction of two or more interactions.

The spatial distribution of the secondary events totaled in column c, Table 2, without any energy discrimination, is given in Fig. 7. This is the projection on a single axis. Figure 8 is the distribution of the secondary event totaled in column h, Table 2, between 90% and full energy of the incident γ ray. Again, the normalization to unity is done only with respect to the accepted events.

These results can only be implemented when the read-out scheme used applies a pulse height selector per wire. The spatial resolution is degraded when the read-out scheme makes its pulse height selection on the total energy deposited (such as in the scintillation detector).

As the energy increases to 500 keV, the fraction of Compton multiple scattering increases (column d). The 90% to full pulse energy selection greatly supresses the pulses due to multiple interactions, i.e., from 35.6% to 19.2% when the thickness is 1.5cm at 500 keV. As expected, the overall detection efficiency drops (in the above case from 33.7% to 22.2%) while the image resolution is greatly enhanced.

5. Spatial Resolution for γ rays – Experimental Results

We have constructed a 5cm×5cm×0.75cm-thick chamber consisting of 25 tungsten wires 3.9 μ in diameter spaced 2mm apart (similar to the chamber shown in Fig. 1). The chamber was made of glass sections glued together with a low vapor pressure epoxy. * We have made preliminary measurements of the spatial resolution, using a Na^{22} source collimated to 0.8mm rms at the chamber. The source was moved with respect to the anode wires by means of a micrometer screw. A single wire was connected to a charge-sensitive amplifier while the other wires were grounded. The chamber was operated in the ionization mode at a voltage of 1000 volts.

The number of counts per unit of time as a function of the micrometer position is shown in Fig. 9. The trigger level was set above the noise. The source provides a profile with an rms deviation from the average of 1.25 mm. By assuming a gaussian distribution for the collimated source, the spatial resolution is unfolded into ~ 1 mm rms, which is approximately equal to that expected for 2mm wire spacing.

6. Modulation Transfer Function

The line spread function gives an indication of the blurring of a line object due to single and multiple interactions. It can be calculated from the data in Table 2 and Figs. 7 and 8 for each gamma-ray energy and each chamber thickness. If we wish to include the effect on chamber resolution of non-zero spacing between the detector read-out wires, it is more convenient to speak in terms of the Modulation Transfer Function (MTF). **

In order to show the relative importance of scattering and non-zero wire spacing, we calculated two MTF's for the case of a 500 keV gamma ray in a 1.5cm-thick xenon detector. The results are shown in Fig. 10. Curve (b) shows the MTF due to scattering alone; curve (a) shows the MTF due to scattering alone but with a $\geq 90\%$ pulse height selection. The pulse height selection is seen to improve the contrast by eliminating most of the multiple interactions. Curve (c) is the MTF for zero scattering but with wires 2mm apart, and curve (d) is likewise for zero scattering but with wire spacing of 0.5mm. In order to find the MTF for a combination of the above effects, one simply multiplies the corresponding MTF for individual contributions.

---

*Some component of this chamber (perhaps the Epoxy) introduced significant electronegative impurities which could not be removed by the field emission clean-up process (ENIP). We are now testing an all-ceramic construction chamber.

** The Modulation Transfer Function is the fourier transform of the line spread function. For further information concerning the Modulation Transfer Function, see reference 11.

As the figure indicates, for wire spacing of 2mm our resolution will be limited by the wire spacing itself, rather than by scattering. For 0.5mm spacing, spatial frequencies as high as 15 cycles/cm still have high modulation. At these high spatial frequencies, (corresponding to resolutions better than 1mm) the image quality will be determined not by the inherent resolution of the xenon detector but by our ability to provide it with enough events per square mm, so that statistical fluctuations from one picture element to the next are not greater than the contrast we are trying to observe.

7. Counting-rate Limitations and Readout

Good spatial resolution alone is not sufficient to construct an acceptable image. A high-counting rate capability permits the use of the short-lived isotopes, allows dynamic studies, and enhances the image quality by improving the statistics.

In the liquid xenon chamber each wire delivers a pulse with a rise time of less than 150 nsec. With proper pulse shaping, a counting rate $> 10^5$ per sec per wire is possible (10 μsec resolving time). A camera handling the electronic signal from each wire independently could provide a counting rate of $n \times 10^5$ C/sec, where n is the number of wires. We can even extend it further to say that if the x-direction is read by the central wires anode, and the y-direction is read from the induced pulse at the one cathode, while ambiguities* are resolved by the second cathode, the maximum counting rate can be $10^5 \times n^2$ C/sec. At this time it is hard to conceive of the fast electronics which could handle such an input, even for a modest number of wires.

In the positron camera, the time resolution is limited by the distance the electrons travel in the liquid. In order to obtain 0.3 μsec coincidence resolution, the electrons should not drift more than 1.0 mm. A possible configuration is one in which the anode is made of several wire planes placed 3 mm apart, with a cathode between adjacent anode planes.

We also note that the signal induced on the cathode (due to the positive charges moving away from the wires) is spread over several wires. The readout scheme must find the center of gravity of this induced pulse.

We have designed and tested a readout scheme that is limited to a rate of 10^6 C/sec and automatically finds the center of gravity of an induced pulse (Fig. 11). Each wire or cathode strip is connected to the adjacent one through a resistor. The current, due to a charge on any of the wires, is divided by the resistor array. The location of the wire is mapped by the ratio of the charge, sensed by the charge-sensitive amplifier at one end, to the total charge deposited. This ratio is performed by a high speed divider, and may be fed directly to an oscilloscope for immediate x-y display.

The initial configuration we built is able to resolve one wire out of 30 for a pulse height range of 25% to 100% of maximum. We developed a thin film nichrome resistive array that was deposited at the ends of the wires to provide ~ 50Ω between them. This is attractive, not only for its simplicity, but because it allows all of the wires to be terminated within the chamber, so that only the two end leads must be brought out.

*Coincidence ambiguity arises when an event at the intersection of any two wires occurs within say, < 1 μsec of another event at another intersection. All four corners of the rectangle appear to have a signal. An additional plane of detection is needed to resolve the ambiguity. The second cathode can be used to provide the diagonal array.

8. Conclusion

We conclude that a liquid xenon radioisotope camera promises many advantages over any other existing γ-ray cameras. Spatial resolution better than 1 mm and counting rates higher than 10^6 C/sec (limited only by the design of the collimator and the cost of the electronics) are possible.

The energy resolution needs to be improved, although the presently achieved 17% FWHM will be sufficient in most cases.

Note added in proof: We have recently achieved an energy resolution of 13% FWHM with a collimated Hg^{203} source using a parallel-plate ionization chamber containing a Frisch grid.

Acknowledgments

We are indebted to Tony Vuletich, Joe Savignano and S. O. Buckingham for their assistance in building and maintaining our equipment and to Ron Jones for his electronic work. We thank Pete Schwemin, Terry Mast, and Sherwood Parker for their contributions. We are especially grateful to Tom Budinger for his interest and useful discussions.

This work was supported in part by the Atomic Energy Commission and in part by the National Aeronautics and Space Administration.

References

1. R. A. Muller, S. E. Derenzo, G. Smadja, D. B. Smith, R. G. Smits, H. Zaklad, and L. W. Alvarez, Phys. Rev. Letters 27, 532 (Aug. 1971).
2. L. Miller, S. Howe, and W. Spear, Phys. Rev. 166, 871 (1968).
3. H. O. Anger, ISA Trans. 5, 311 (1966).
4. W. H. McMaster et al., Lawrence Radiation Laboratory Report UCRL-50174, Sec. II, Rev. 1, May 1969.
5. J. H. Hubbell, Photon Cross Sections, NSRDS-NBS 29, Aug. 1969.
6. R W. F. Miller, J. Reynolds, and W. J. Snow, Rev. Sci. Instr. 28, 717 (1957).
7. L. Lavoie, Positron Detection System Using Liquid Xenon Scintillator, in Proc. Soc. Nucl. Medicine, 18th Annual Meeting, June 1971.
8. H. Zaklad, Lawrence Radiation Laboratory Report UCRL-20690, April 1971.
9. W. R. Binns, Washington University, St. Louis, private communication.
10. L. Miller, Lawrence Berkeley Laboratory, Berkeley, private communication.
11. Photoelectric Imaging Devices, edited by L. M. Biberman and Sol Nudelman (Plenum Press, New York, 1971).

Table 1

Comparison of NaI(Tl), germanium and liquid xenon for 500 keV gammas

	Usable initial pulse (A) (electrons)	Energy resolution (FWHM)	Photofraction $\frac{\sigma_p}{\sigma_p + \sigma_c}$ (C)	Photoelectron absorption length (cm)	Cost ($/cm^3)
NaI(Tl)	1,500	11%	0.19	15.7	1
Germanium	170,000	≈1%	0.046	52.0	110 (D)
Liquid xenon	22,000	17% (B)	0.24	15.7	5

(A) Electrons due to ionization in Ge and liquid xenon, or those converted to photoelectrons in the photocathode of the NaI(Tl). This value (when modified by the Fano factor) controls the statistical fluctuations.

(B) Present state for 279 keV γ's. FWHM due to 5.5 MeV α's is better than 13%.

(C) σ_p is the photoelectric cross section and σ_c is the Compton cross section.

(D) High purity Ge, available from General Electric Corp.

TABLE 2

ESTIMATED PROBABILITY FOR VARIOUS PROCESSES IN LIQUID XENON

	WITHOUT ENERGY DISCRIMINATION				90% ENERGY DISCRIMINATION			
		UNITY AREA**				UNITY AREA**		
ENERGY (KEV)	(a)* GROSS DETECTION EFFICIENCY	(b) SINGLE PHOTO ELECTRIC	(c) SINGLE COMPTON AND ESCAPE	(d) TWO OR MORE INTERACTIONS	(e)* DETECTION EFFICIENCY	(f) SINGLE PHOTO ELECTRIC	(g) SINGLE COMPTON AND ESCAPE	(h) TWO OR MORE INTERACTIONS
				CHAMBER THICKNESS = .75 CM				
100	98.5	94.1	0.8	5.1	97.2	97.7	0	2.3
200	53.6	71.8	11.2	17.0	47.5	94.6	0	5.4
500	18.6	22.6	47.4	30.0	9.7	88.0	0	12.0
1000	11.9	7.6	73.3	19.1	3.1	85.2	0	14.8
				CHAMBER THICKNESS = 1.5 CM				
100	99.97	94.1	0.8	5.1	98.7	97.2	0	2.3
200	78.4	71.8	8.7	19.5	71.8	92.6	0	7.4
500	33.7	22.6	41.8	35.6	22.2	80.8	0	19.2
1000	22.4	7.6	68.6	23.8	9.2	75.4	0	24.6
				CHAMBER THICKNESS = 3.0 CM				
100	100	94.1	1.2	5.1	98.8	97.7	0	2.3
200	95.3	71.8	6.4	21.8	89.2	91.2	0	8.6
500	56.1	22.6	22.4	55.0	43.6	73.3	0	26.7
1000	39.8	7.6	40.4	52.0	23.0	63.7	0	36.3

* NORMALIZED TO THE INCIDENT RADIATION.

** NORMALIZED SUCH THAT THE SUM OF COLUMNS b, c, d OR f, g, h IS EQUAL TO 100%.

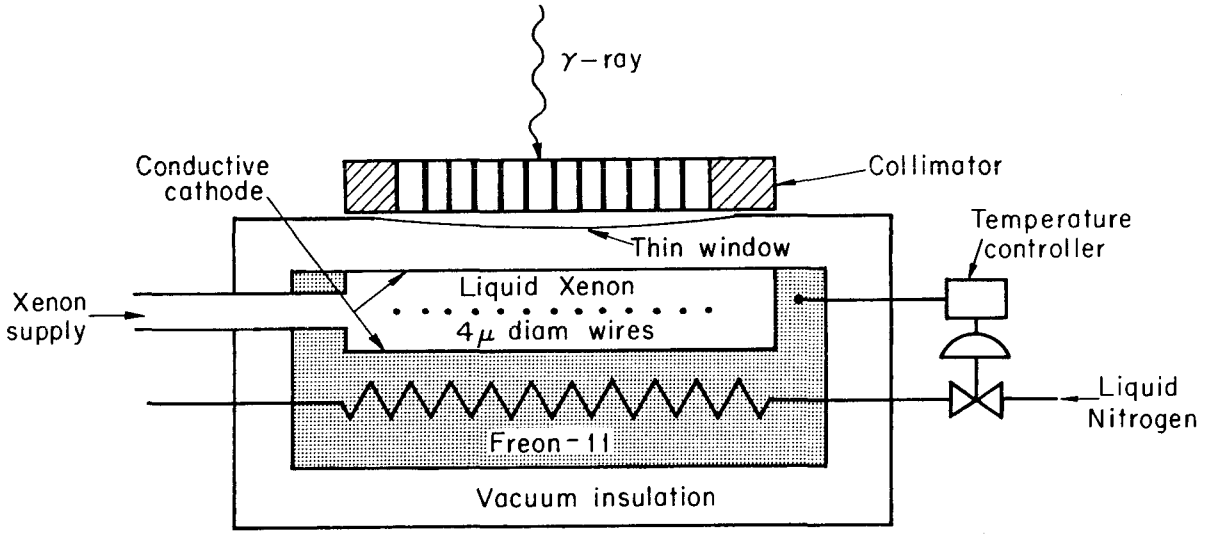

XBL722-2348

Fig. 1. Detector section of the liquid xenon radioisotope camera under development. The γ rays are converted in the liquid xenon, and the ions are collected (and multiplied) on the 4μ-diameter anode wires. Two dimensional imaging is achieved by reading the induced pulse off of an array of cathode strips perpendicular to the anode wires. Liquid xenon temperature is maintained by a freon-11 bath and a liquid nitrogen heat exchanger. This figure is not to scale.

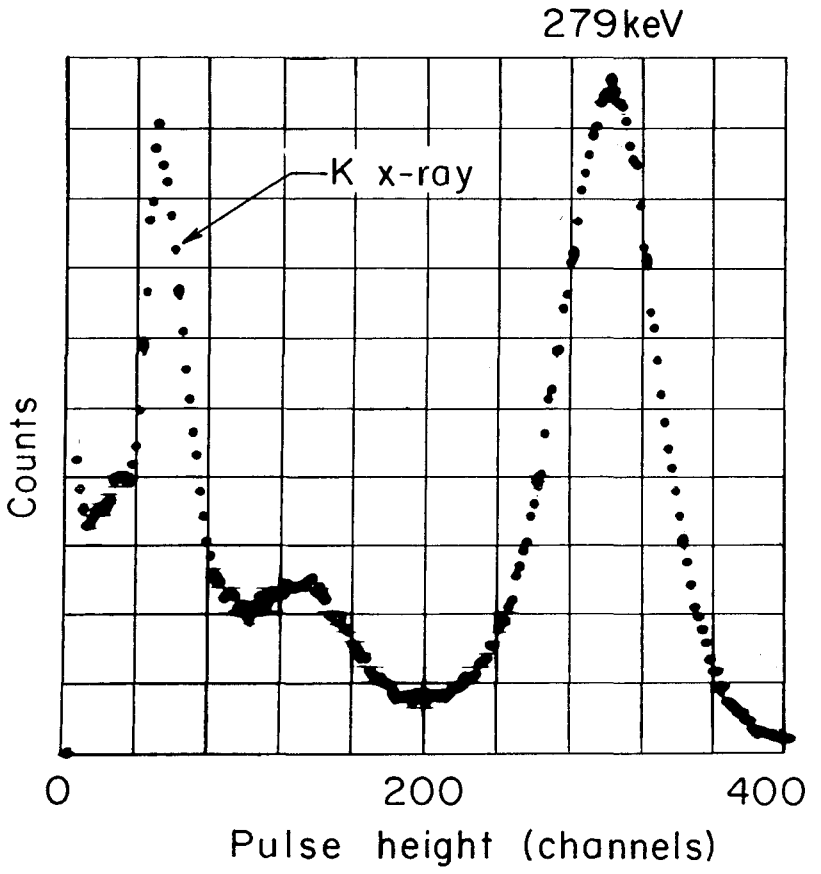

XBL722-2248

Fig. 2. Pulse height spectrum for a colliminated Hg^{203} source in liquid xenon. The gain in the liquid is 10. The FWHM of the 279 keV peak is 22%

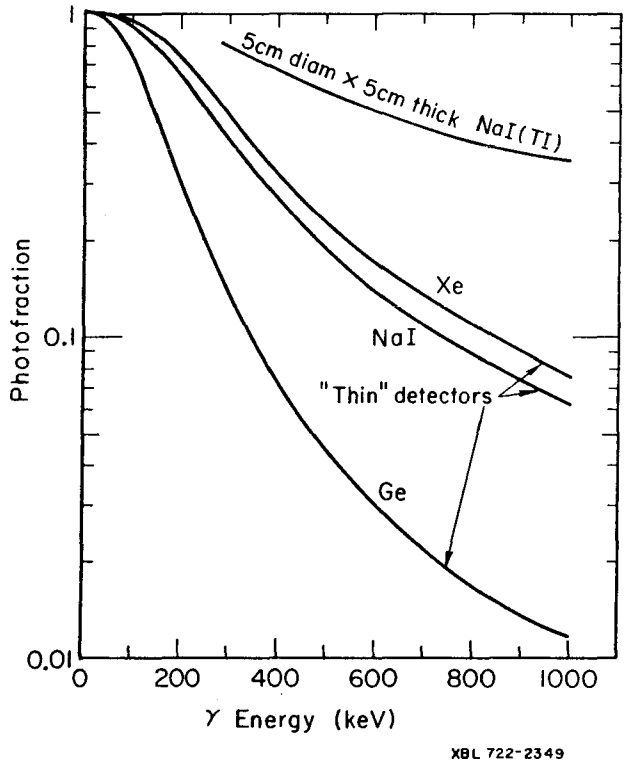

Fig. 3. Photofraction (the fraction of the photopeak to total) for "thin" Xe, NaI, and Ge detectors based on the ratios of the cross sections $\sigma_p/(\sigma_p+\sigma_c)$. For a thick detector, a larger fraction of the events produce full pulse height and fall into the photopeak. An example is given for 5 cm dia X 5cm thick NaI (T1).

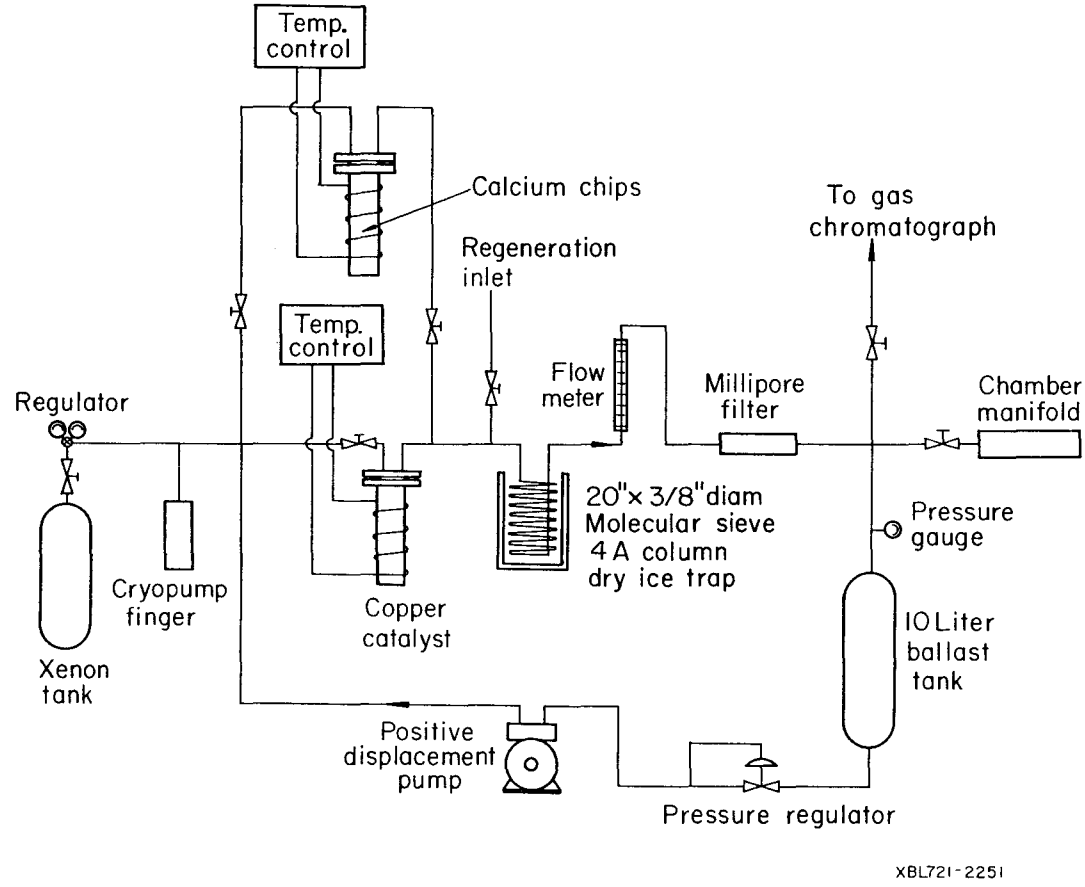

Fig. 4. Gas purifier: Xenon gas continuously circulates by means of the pump. A copper catalyst is maintained at 200°C and the molecular sieve 4A at dry ice temperature. Periodically, the calcium (600°C) reactor is switched in.

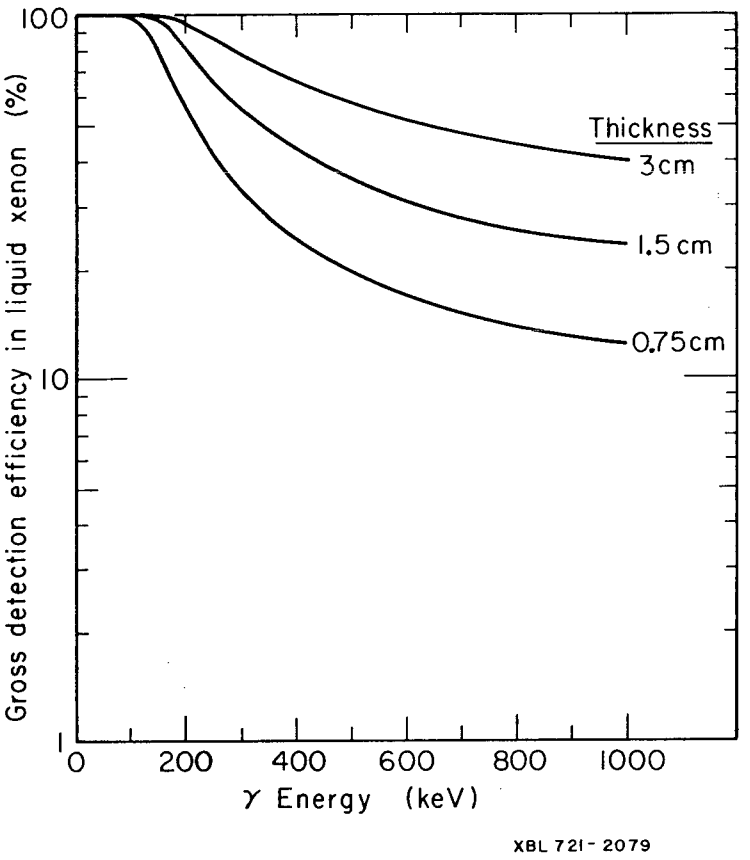

Fig. 5. Gross detection efficiency (Compton plus photoelectric) for various thicknesses of liquid xenon detectors.

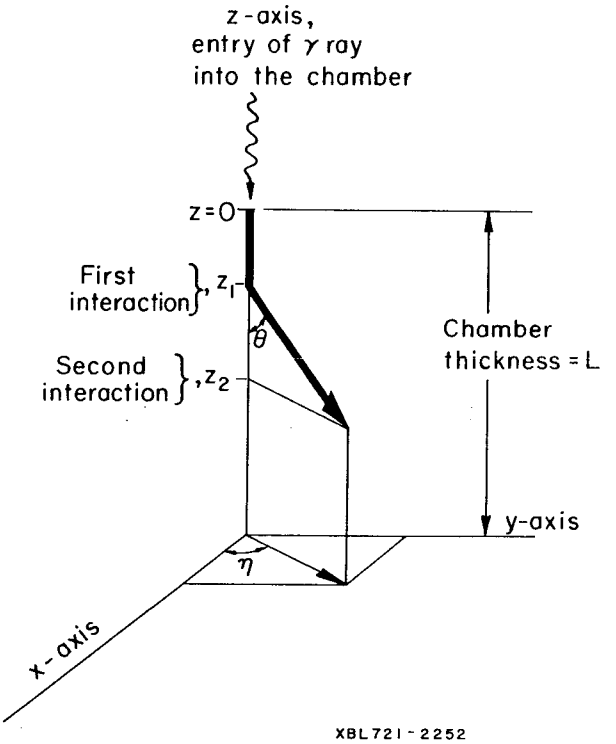

Fig. 6. Projected path (on the y axis) of the incoming γ ray, used in the calculation of the probability of spatial distribution in liquid xenon.

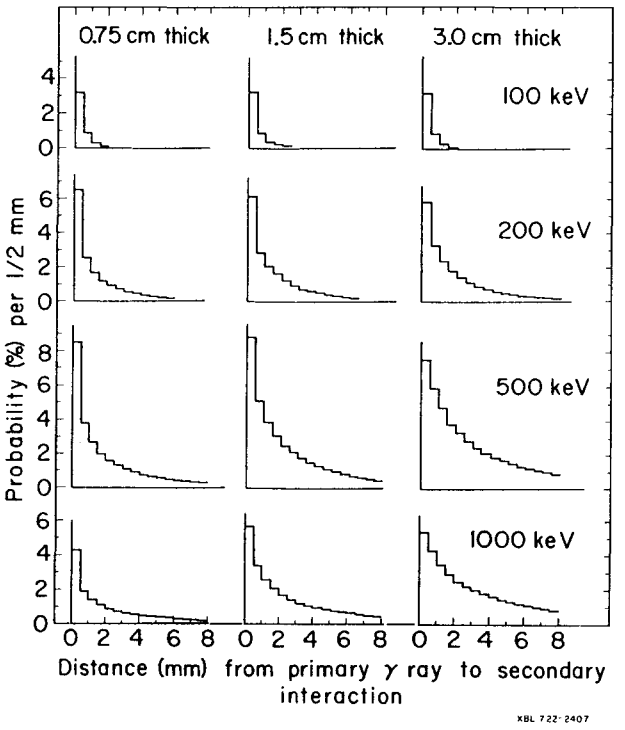

Fig. 7. Calculated loss of resolution in liquid xenon due only to multiple scattering. Projected single Compton and primary photoelectric processes not shown here, (see Table 2, col. b, c) are assumed to fall in the first 1/2 mm. This is the projected error on a single axis.

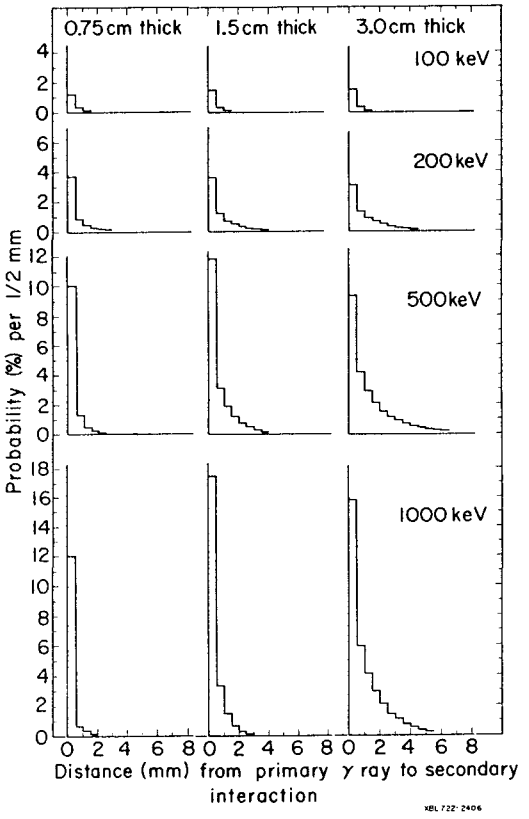

Fig. 8. Calculated loss of resolution in liquid xenon due only to multiple scattering, when a pulse height selection of 90% to 100% of full pulse height is detected on each wire. Primary photoelectric (not shown) (see Table 2, col. f) are assumed to fall in the first 1/2mm. This is the projected error on a single axis.

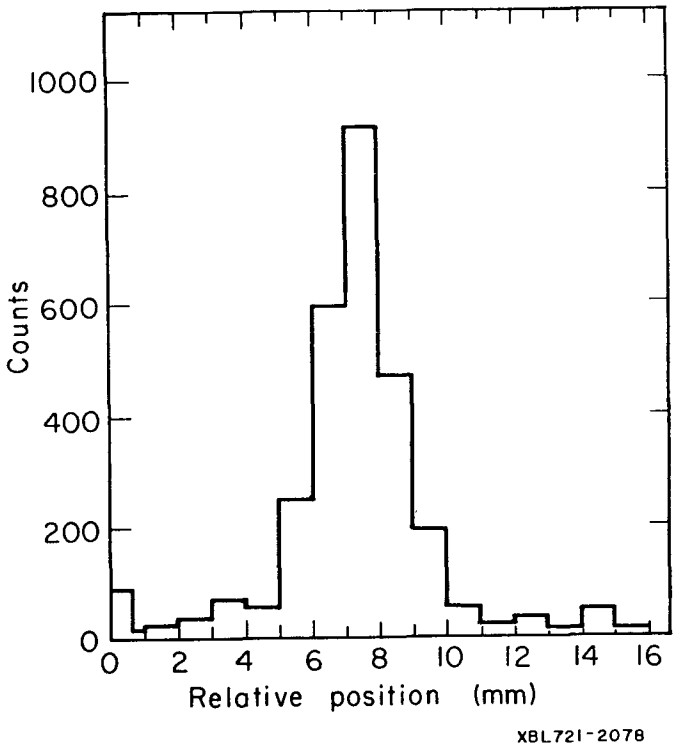

Fig. 9. Image of a collimated Na^{22} source on a single wire, detected in a 0.75 mm-thick liquid xenon chamber. The chamber contains 25 wires spaced 2 mm apart. The source was moved by means of mechanical screw. A background of 60 counts has been subtracted.

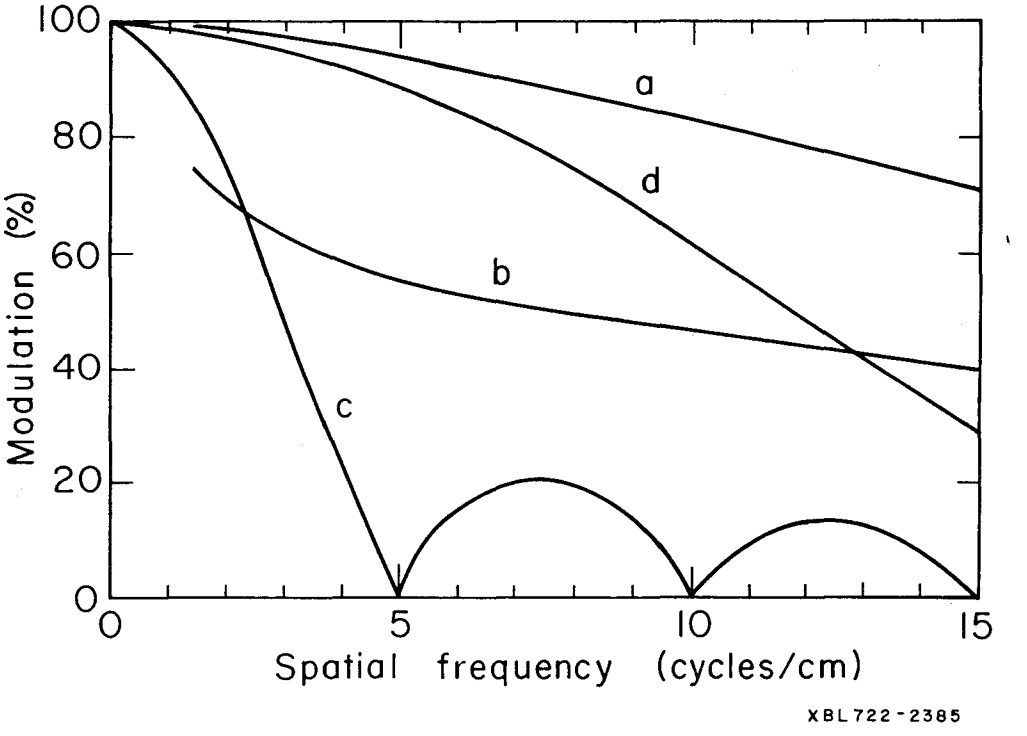

Fig. 10. MTF for scattering of 500 keV γ rays in a 1.5 cm-thick liquid xenon chamber (a: > 90% pulse height selection, b: no pulse selection) and for discrete nature of wires (c: 2mm spacing, d: 0.5 mm spacing). Curves a and b do not extend below spatial frequencies of 1.5 cycles/cm due to computational difficulties.

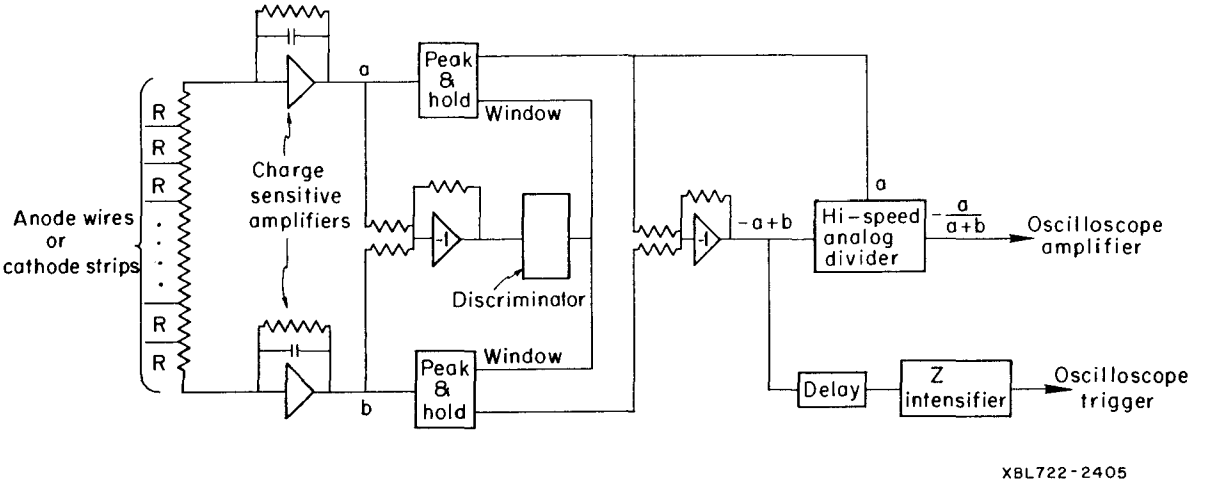

Fig. 11. Schematic diagram for a one dimensional charge ratio readout. (a + b) is the total charge deposited while $\frac{a}{(a+b)}$ is the position. The peak and hold modules are necessary in order to minimize the effects of parasitic capacitance. The division is performed by an Analog Devices Model 422J.